Supporting Information

Controlled Reconstruction of Metal-Organic Frameworks via Coordination Environment Tuning as Oxygen Evolution Electrocatalysts

Jiangli Gong,[a,c]‡ Qianglong Qi,[a,b]‡ Zhiyuan Wang,[a,b] Guangxin Zhao,[a,b] Jianliang Yuan,[a,c] Chengxu Zhang[a*] and Jue Hu[a,b,d*]

[a]Faculty of Metallurgical and Energy Engineering, Kunming University of Science and Technology, Kunming, China

[b]Key Laboratory of Unconventional Metallurgy, Kunming University of Science and Technology, Kunming, Yunnan, China

[c]LuXi KuoBo Precious Metals Co. Ltd., Honghe, Yunnan, China

[d]Southwest United Graduate School, Kunming, P. R. China

‡These authors are contributed equally

[*]Corresponding authors: chxzhang@kust.edu.cn, hujue@kust.edu.cn

Experimental Section

Materials

Cobalt nitrate hexahydrate, Nickel nitrate hexahydrate, Sodium hydroxide, p-Phthalic acid, 4,4'-Bipyridine from Aladdin Corporation. All of the above chemicals were of analytical grade and used as received without further purification. Commercial nickel foams (NF, nickel content: 99.8 %) were purchased from Taiyuan Liyuan Lithium Battery Technology Co. Ltd. and cut into small pieces having a geometric area of 1 cm × 3 cm. NF was first ultrasonicated in 0.5 M H_2SO_4 (Sigma-Aldrich) for 1 h, and then washed with deionized water alternately three-time, and dried at room temperature. All the above chemicals were of analytical grade and used as received without further purification. Ultrapure deionized water (DI, 18.2 MΩ cm^{-1}) was used in all experiments. Commercial nickel foam (NF, thickness: 1.7 mm) was purchased from Taiyuan Liyuan Lithium Battery Technology Co. Ltd. and cut into small pieces with a geometric area of 1 cm×3 cm. NF was first ultrasonicated in 0.5 M H_2SO_4 for 1 h to remove the thin oxide layer formed on the surface, and then washed with deionized water alternately three times, followed by drying at room temperature.

Characterizations

Field-emission scanning electron microscopy (FESEM) imaging was carried out using a Nona-Nano SEM450 at an accelerating voltage of 5 kV. Transmission electron microscopy (TEM), high-resolution TEM (HRTEM), and high-angle annular dark-field scanning transmission electron microscopy combined with energy-dispersive X-ray spectroscopy (HAADF-STEM-EDX) were conducted on a Tecnai G2 TF30 operating at 300 kV. The powder X-ray diffraction (XRD) patterns were recorded employing a Rigaku D/Max-2200 PC diffractometer, within the diffraction angle range of 2θ = 5-80°, utilizing Cu Kα radiation (λ = 1.5418 Å) at a voltage of 40 kV and a current of 40 mA. X-ray photoelectron spectroscopy (XPS) measurements were conducted on a PerkinElmer PHI 5500 XPS system, featuring a resolution of 0.3-0.5 eV, sourced from a monochromated aluminum anode with Mo Kα radiation (1486.6 eV). The XPS spectra were calibrated against the C 1s peak of adventitious carbon at 284.80 eV. The electrochemical Raman measurements were carried out on a confocal LabRAM Soleil

Raman Microscope Raman system (HORIBA FRANCE SAS). A Nd-YAG laser with 532 nm excitation wavelength and a 50× microscope objective with a numerical aperture of 0.55 were used in all measurements. Raman frequency was calibrated by a standard silicon (Si) wafer to 520.7 cm^{-1} during each experiment. In-situ electrochemical Raman experiments were employed in a Raman cell, and an electrochemical workstation CHI 760E potentiostat was used to control potential. Raman curves were recorded from 200 to 2000 cm^{-1}. Operando Raman spectra were performed using an open spectroelectrochemical cell consisting of a three-electrode system. A calibrated Hg/HgO (1 M KOH) electrode and a Pt plate were served as the reference and counter electrodes, respectively.

Electrochemical Measurements

Electrochemical measurements of the as-synthesized samples were performed with a CHI760E electrochemistry workstation (CH Instruments, Inc.) using a standard three-electrode electrochemical cell with Pt sheet and Hg/HgO as the counter electrode and the reference electrode, respectively. 50 μL of the catalysts ink was loaded on a clean NF electrode (NF, 0.5 cm^2) by drop coating to form the electrode, and dried slowly at room temperature. The final mass loading of the catalysts on electrode is around 1 mg cm^{-2}. The electrochemical measurements were all performed at room temperature, and the potential was referenced to that of the reversible hydrogen electrode (RHE). For the RHE calibration, the potential difference between Hg/HgO and RHE was measured in 99.999% pure H_2 saturated 1.0 M KOH aqueous solution. During the measurement, high-purity H_2 is bubbled into the electrolyte to saturate the electrolyte and fix the reversible hydrogen potential. Cyclic voltammograms (CV) were taken several cycles to bubble away the surface contaminates and at the same time stabilize the catalysts. The polarization curves were obtained by linear sweeping with a scan rate of 1 mV s^{-1} in O_2-saturated 1.0 M KOH aqueous solution. Double layer capacitance (C_{dl}) was estimated by the CV cures at various scan rates (10-50 mV) in the potential region of 0.1-0.2 V *vs.* RHE. All the polarization curves were iR-corrected, except as otherwise noted. Electrochemical impedance spectroscopy (EIS) is recorded at an applied potential of 1.53 V *vs.* RHE from 100 kHz to 0.1 Hz. Chronopotentiometry (CP)

responses curve was performed under a high constant current density of 100 mA cm^{-2} in 1.0 M KOH using carbon rod as the counter electrode at room temperature.

Supplementary Figures

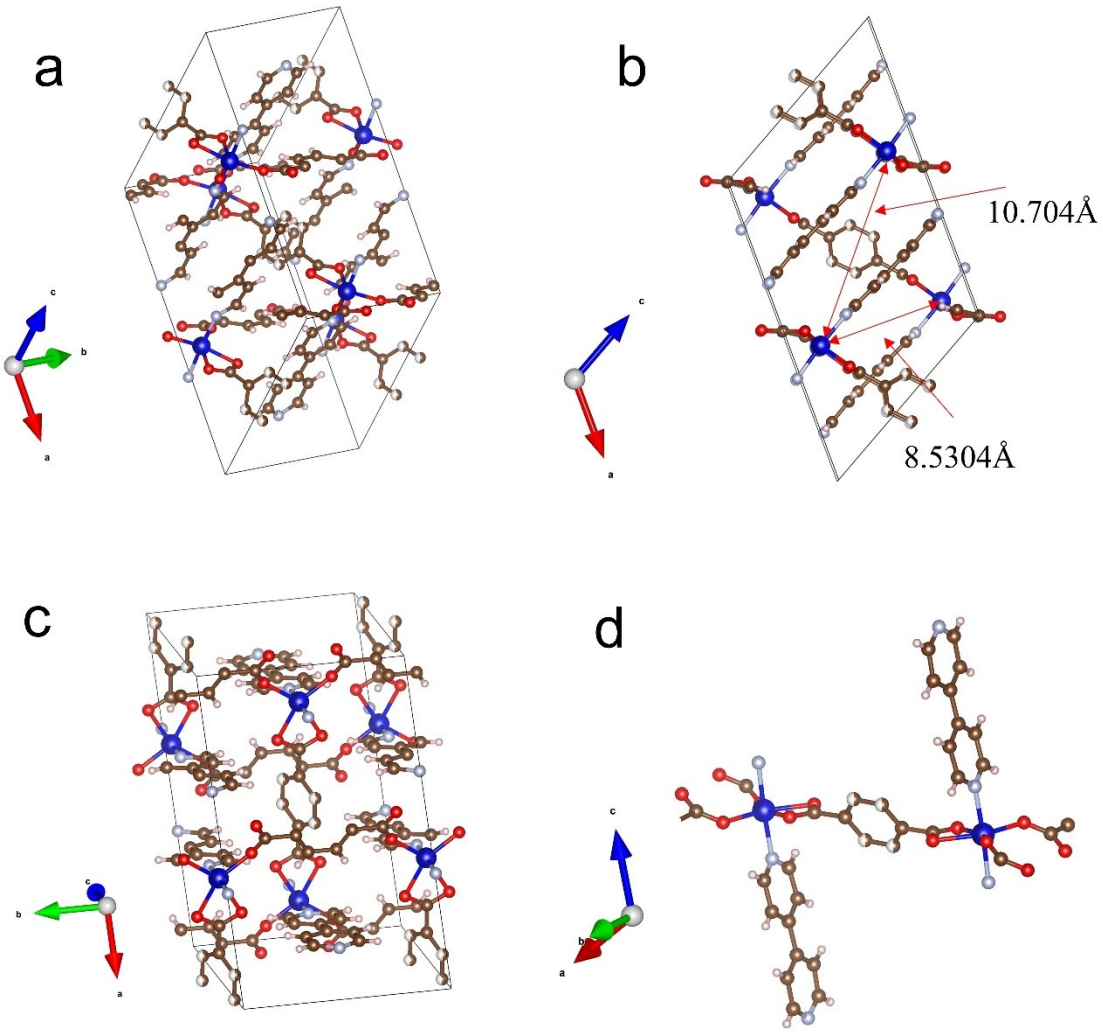

Figure S1. The schemes to create MOF structures.

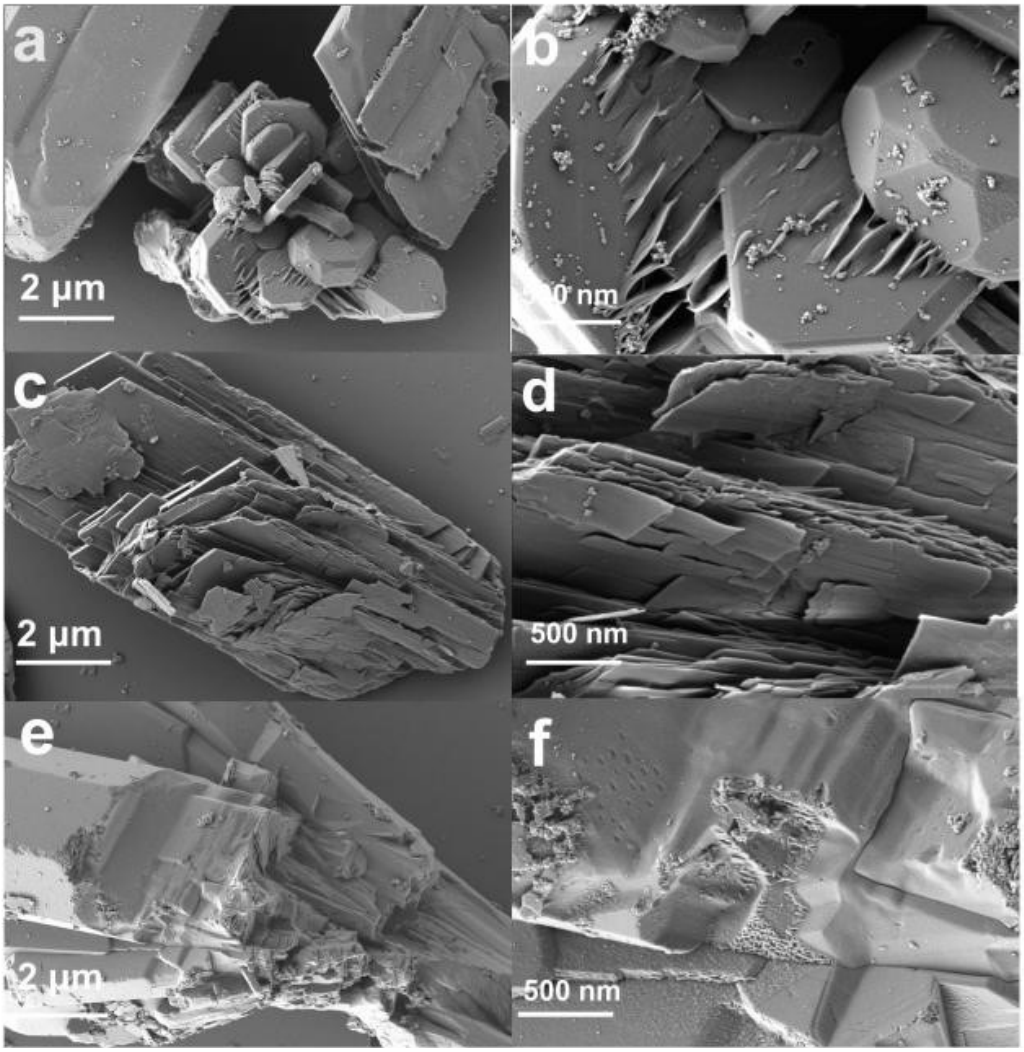

Figure S2.SEM images of (a) Co-MOF, (b), Ni-COF and (c) CoNi-MOF catalyst.

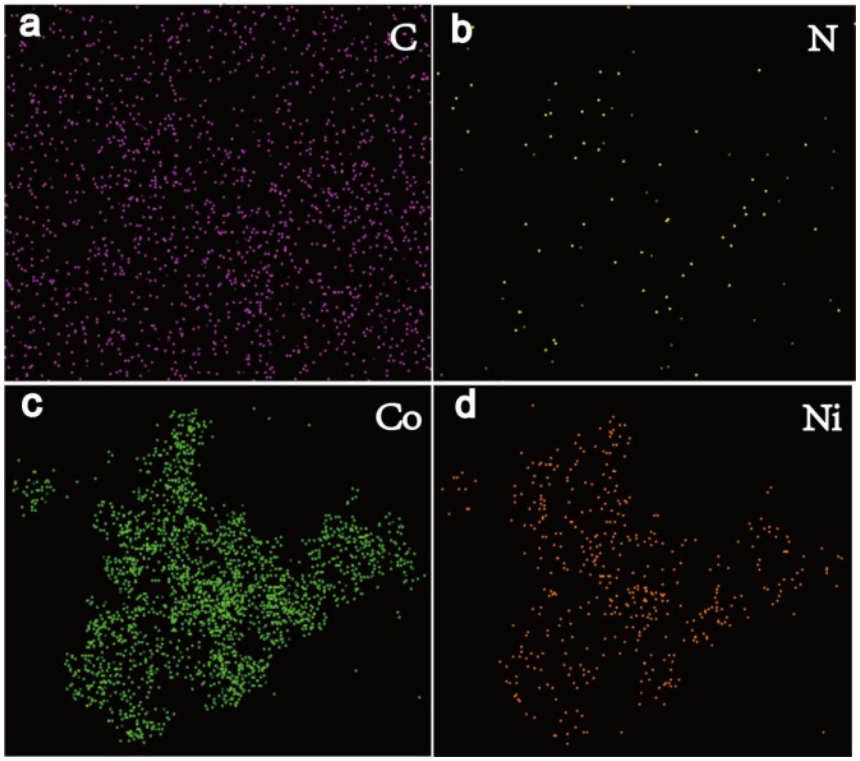

Figure S3. EDS profiles of CoNi-MOF catalysts (a) C elemental distribution profile, (b) N elemental distribution profile, (c) Co elemental distribution profile, (d) Ni elemental distribution profile

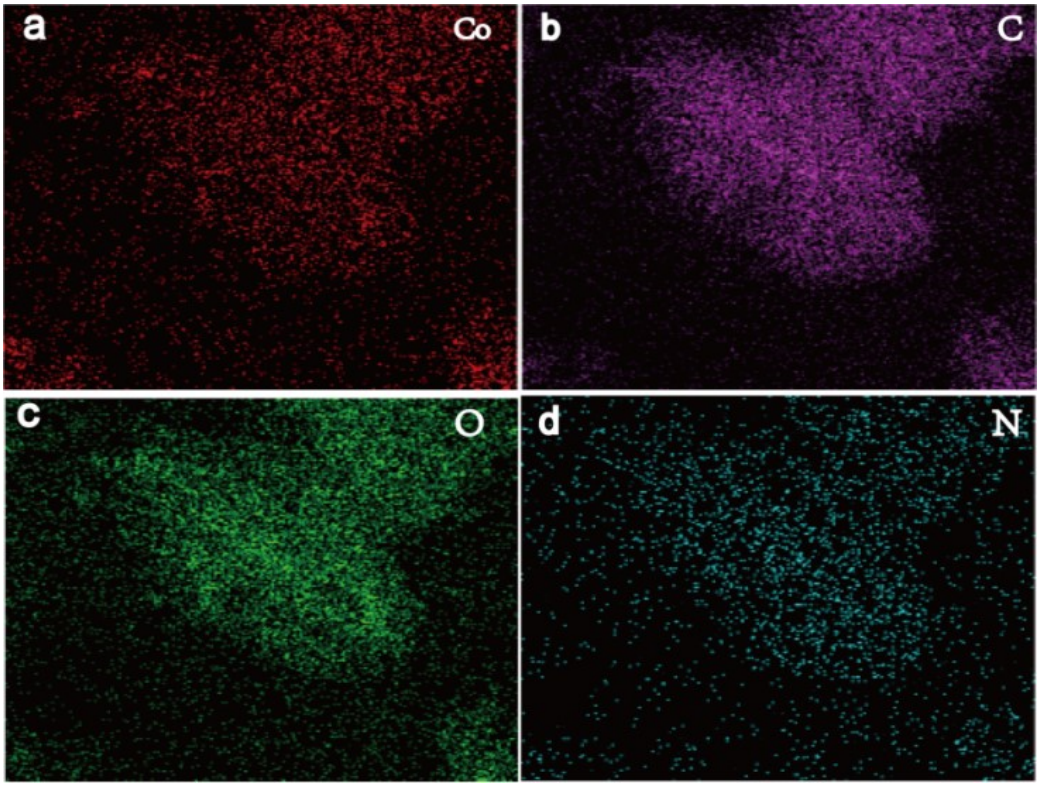

Figure S4 EDS profiles of Co-MOF catalyst with (a) Co elemental distribution profile, (b) C elemental distribution profile, (c) O elemental distribution profile, and (d) N elemental distribution profile.

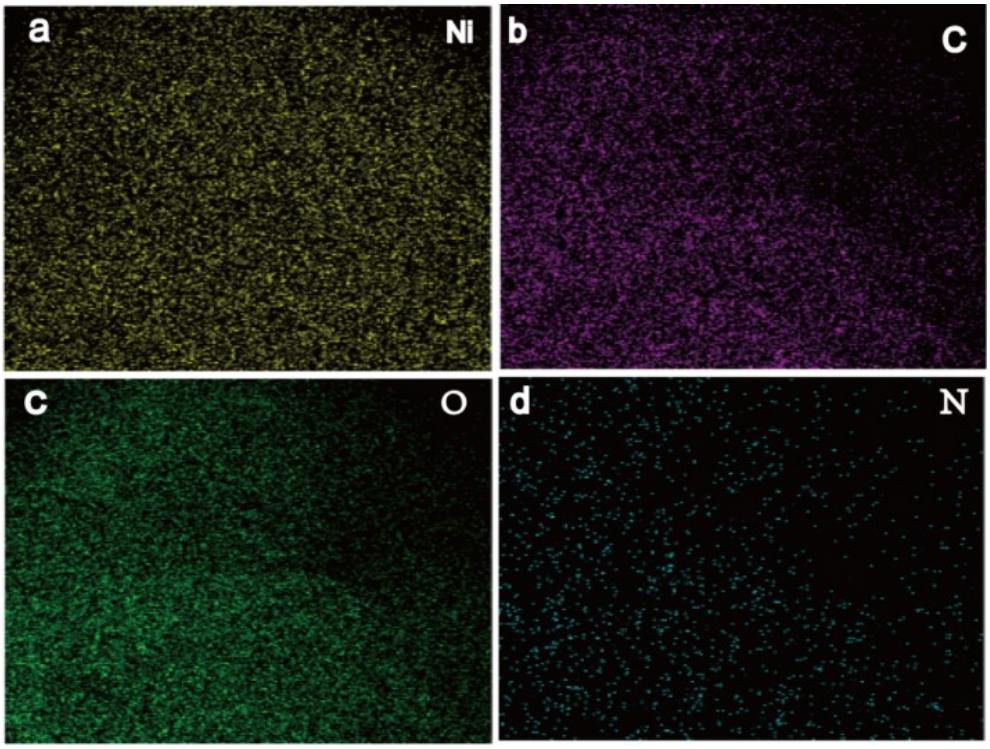

Figure S5 EDS profiles of Ni-MOF catalysts (a) C elemental distribution profile, (b) N elemental distribution profile, (c) Co elemental distribution profile, (d) Ni elemental distribution profile

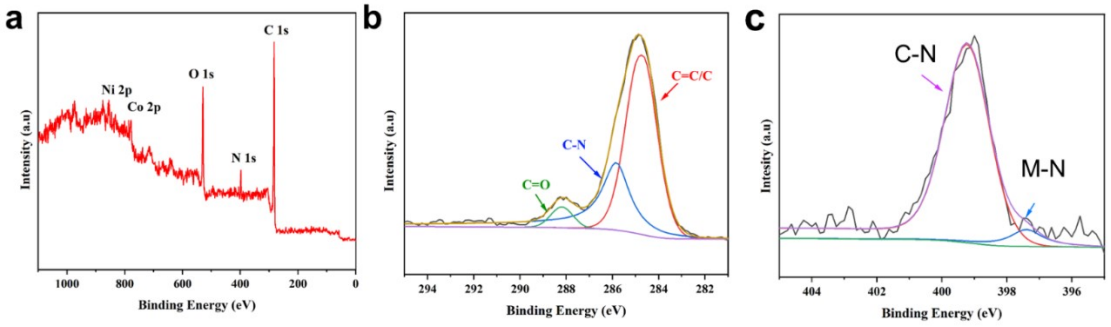

Figure S6 CoNi-MOF XPS (a) full spectrum, (b) C1s, (c) N1s

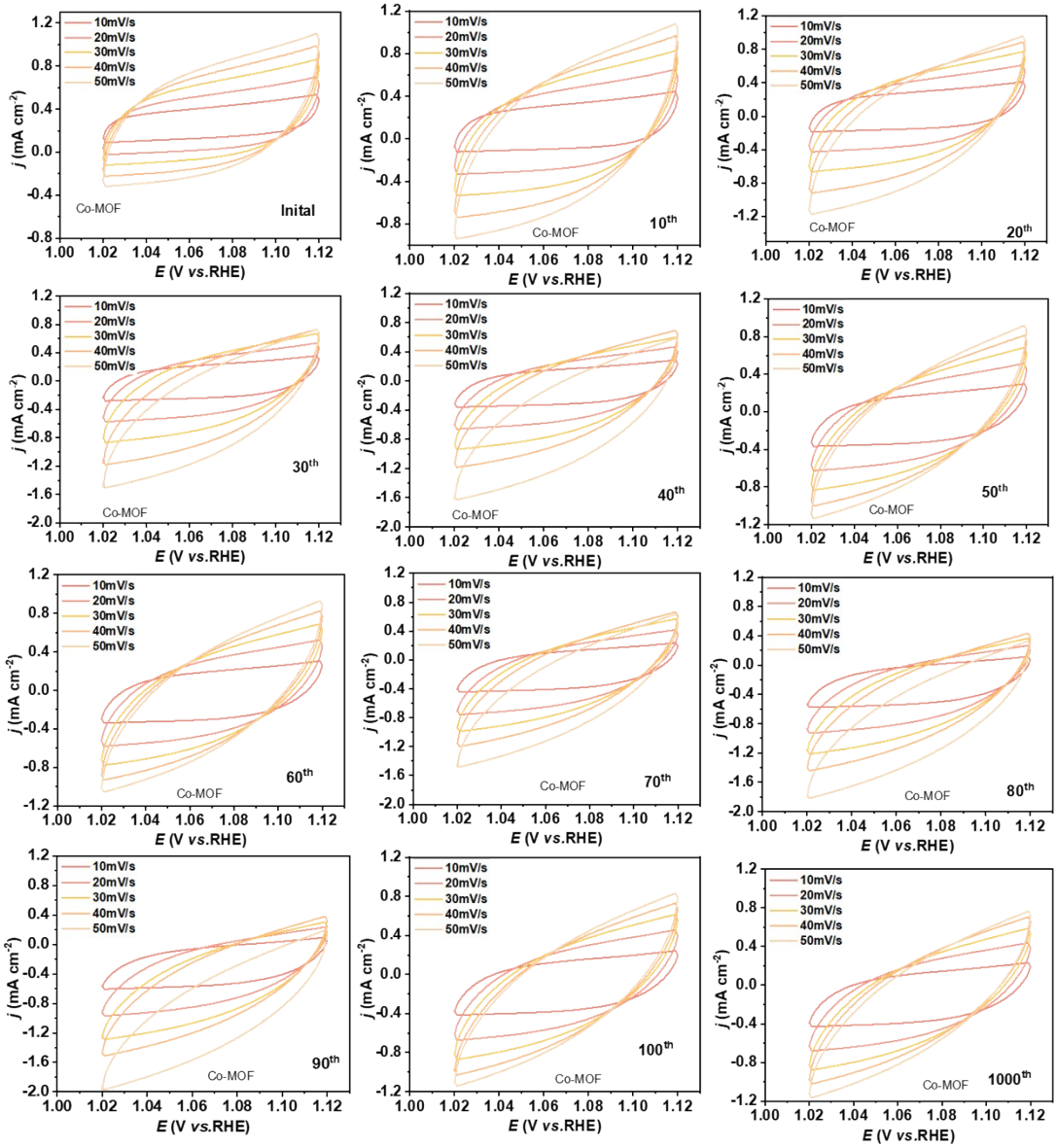

Figure S7 CV curves of Co-MOF precatalysts after different cycles.

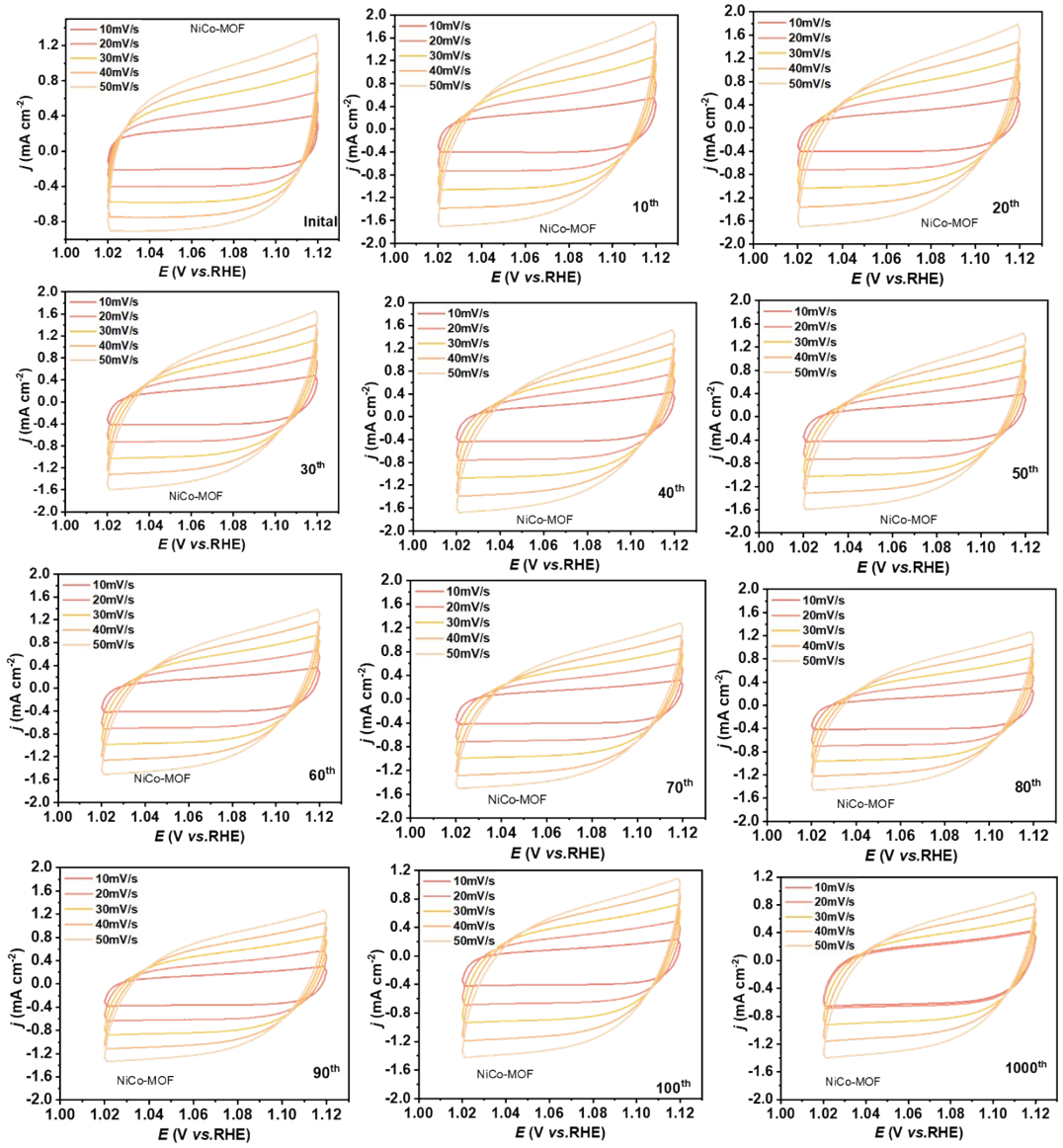

Figure S8 CV curves of NiCo-MOF precatalysts after different cycles.

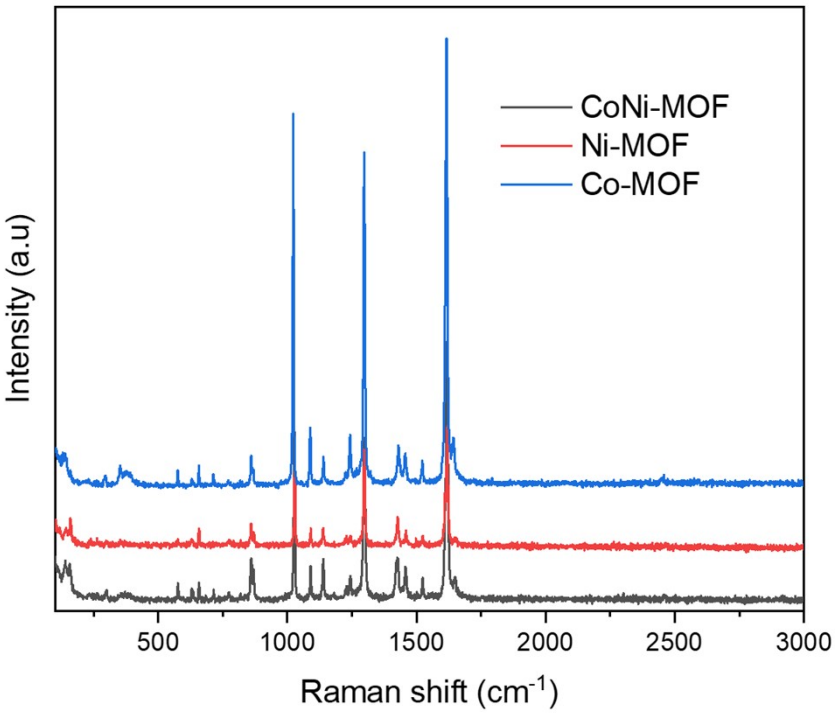

Figure S9. Raman spectrum of Ni-MOF, Co-MOF, and CoNi-MOF.

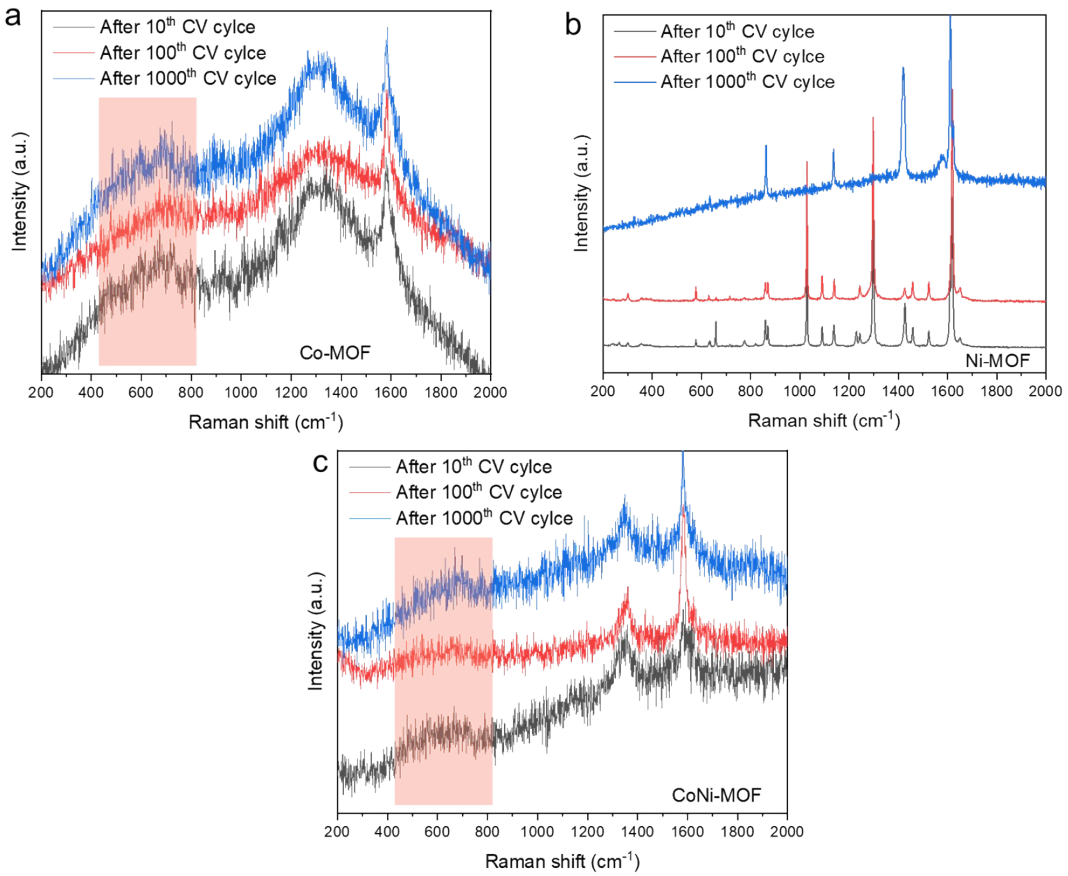

Figure S10. (a) Raman spectrum of Co-MOF after 10th, 100th, and 1000th CV cycles. (b) Raman spectrum of Ni-MOF after 10th, 100th, and 1000th CV cycles. (c) Raman spectrum of CoNi-MOF after 10th, 100th, and 1000th CV cycles.

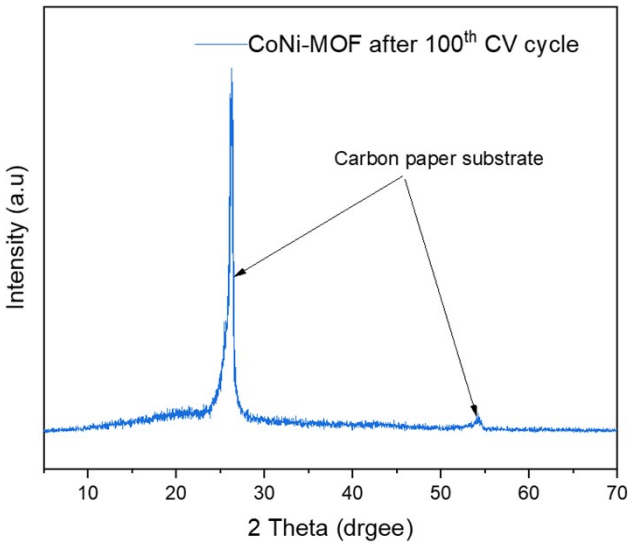

Figure S11. XRD patterns of CoNi-MOF after 100th CV cycles.

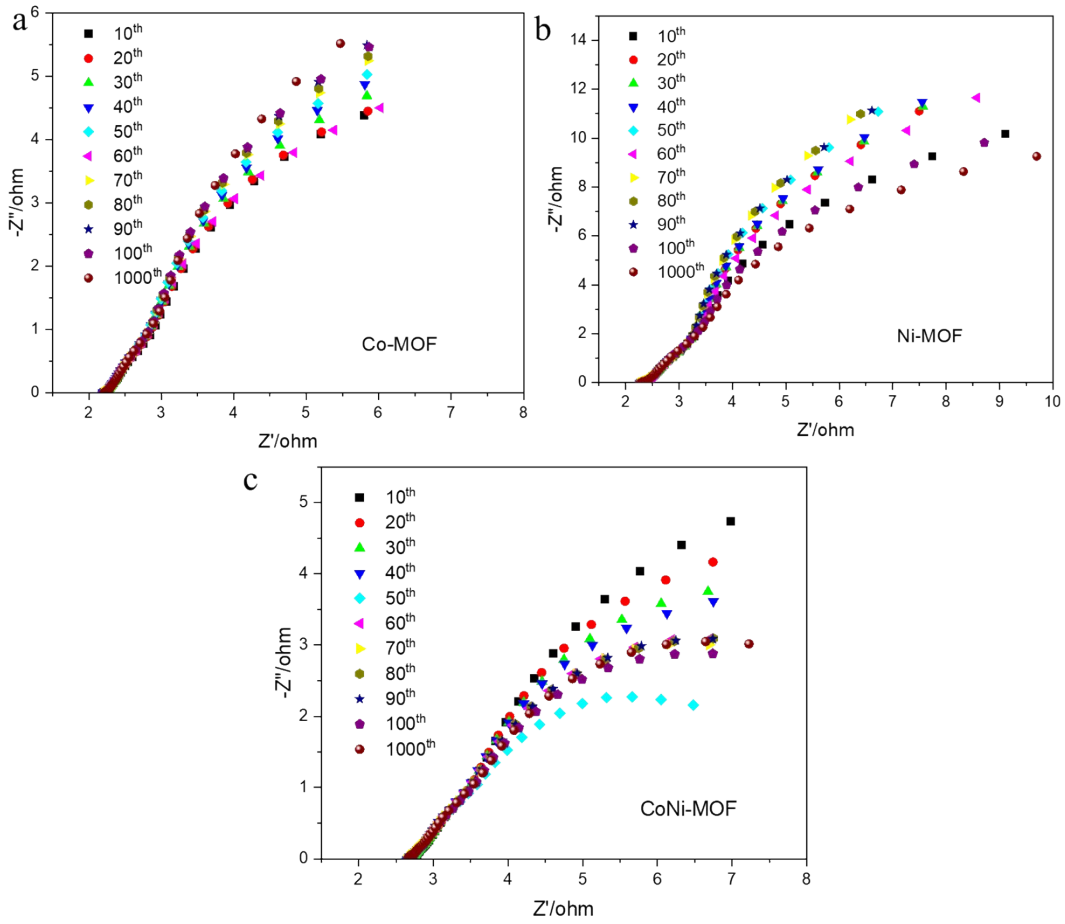

Figure S12. Nyquist plots of (a) Co-MOF, (b) Ni-MOF, and (c) CoNi-MOF precatalysts after different CV cycles for 1.53V vs. RHE.

Supplementary Table

Table S1 C_{dl} of Co-MOF, NiCo-MOF precatalysts after different CV cycles.

CV cycles	Co-MOF (mF cm^{-2})	NiCo-MOF(mF cm^{-2})
Initial	2.37	12.85
10^{th}	11.21	20.67
20^{th}	12.45	22.41
30^{th}	12.60	21.45
40^{th}	12.33	22.57
50^{th}	12.05	21.98
60^{th}	11.78	21.55
70^{th}	10.90	20.80
80^{th}	11.01	20.45
90^{th}	9.98	19.91
100^{th}	10.12	23.66
1000^{th}	10.31	23.78